

Aided Inertial Navigation with Geometric Features: Observability Analysis

Yulin Yang and Guoquan Huang

Abstract—In this paper, we perform observability analysis for inertial navigation systems (INS) aided by generic exteroceptive range and/or bearing sensors with different geometric features including points, lines and planes. While the observability of vision-aided INS (VINS, which uses camera as a bearing sensor) with point features has been extensively studied in the literature, we analytically show that the same observability property remains if using generic range and/or bearing measurements, and if global measurements are also available, as expected, some unobservable directions dismiss. We study in-depth the effects of four degenerate motions on the system observability. In particular, building upon the observability analysis of the aided INS with point features, we perform observability analysis for the same system but with line and plane features, respectively, and show that there exist 5 (and 6) unobservable directions for a single line (and plane) feature. Moreover, we, for the first time, analytically derive the unobservable directions for the cases of multiple lines/planes. We validate our analysis through Monte Carlo simulations.

I. INTRODUCTION AND RELATED WORK

Over the past decades, an inertial navigation system (INS) using an inertial measurement unit (IMU) is among the most popular approaches to estimate the 6 degrees-of-freedom (DOF) position and orientation (pose) in 3D, especially in GPS-denied environments such as underwater, indoor, in the urban canyon, and in space. However, simple integration of IMU measurements that are corrupted by noise and bias, often results in unreliable estimates in a long term, although a high-accuracy IMU exists but remains prohibitively expensive for widespread deployment. A camera that is small, light-weight, and energy-efficient, provides rich information about the perceived environment and serves as an idea aiding source for INS, i.e., vision-aided INS (VINS) [1]–[8]. Nevertheless, many other exteroceptive sensors such as LiDAR [9], RGBD camera [10] and 2D imaging sonar [11], can also be used to aid INS by providing range and/or bearing measurements to features. To date, various algorithms are available for aided INS problems, among which the EKF-based approaches remain arguably the most popular, for example, observability constrained (OC)-EKF [1], [12], and multi-state constrained Kalman filter (MSCKF) [3], [13].

As system observability plays an important role in developing consistent state estimation [14], the observability of VINS has been extensively studied. In particular, the authors

This work was partially supported by the University of Delaware (UD) College of Engineering, the UD Cybersecurity Initiative, the NSF (IIS-1566129), and the DTRA (HDTRA1-16-1-0039).

The authors are with the Department of Mechanical Engineering, University of Delaware, Newark, DE 19716, USA. Email: {yuyang, ghuang}@udel.edu

of [15], [16] examined the system's indistinguishable trajectories. By employing the concept of continuous symmetries, [17], [18] showed explicitly that the IMU biases, 3D velocity, and absolute roll and pitch angles in VINS are observable. In [1], [19], observability analysis for the linearized VINS was performed by analytically finding the right null space of the observability matrix. The corresponding nonlinear observability analysis [20] was also carried out, respectively, for monocular vision-aided INS [2] and RGBD-aided INS [21], where the unobservable directions were found analytically. Previous work shows that there are 4 unobservable directions (3 correspond to global translation and 1 to global yaw) for VINS. However, few have studied the observability for INS aided with generic range and/or bearing measurements using different geometric features. Note that aided INS might be fed into global measurements, such as altitude measurements by barometers and orientation measurements by compasses. It is important to understand the effects of such measurements on the system observability. Moreover, it is of practical significance to examine the degenerate motions that may ruin the system observability properties by causing more unobservable directions (e.g., see [22]).

While most current VINS algorithms focus on using point features [1]–[3], line and plane features are to prevail [10], [23]–[25], because of their advantages: (i) There are plenty of straight lines and planes in common urban or indoor environments (e.g., doors, walls, stairs); (ii) They can be easily detected and tracked continuously over a relatively long time period; (iii) They are more robust in texture-less environments compared to points. In particular, Kottas et al. [25] represented the line with a quaternion and a scalar, and studied the line observability based on this representation with linearized observability matrix. Guo et al. [10] and Panahandeh et al. [24] analyzed the observability of VINS with plane features, while assuming plane orientation is *a priori* known. In contrast, in this work, we make no assumption for lines or planes and advocate to use the orthonormal representation [26] to model the error states for line features. Specifically, the main theoretical contributions of this paper are the following:

- We generalize the VINS observability analysis to INS aided with any type of exteroceptive sensors such as 3D LiDAR, 2D imaging sonar, and stereo cameras, and analytically show that the same observability properties remain (i.e., four unobservable directions).
- We study in-depth the effects of global measurements on the system observability, showing that they, as expected,

will improve the system observability.

- By employing the spherical coordinates for the point feature, we identify 4 degenerate motions that cause the aided INS to have more unobservable directions.
- We perform observability analysis for the aided INS with line and plane features, respectively, and show that there exist 5 (and 6) unobservable directions for a single line (and plane) feature. Moreover, we analytically derive the unobservable directions for multiple lines (planes), without any assumption about features.

II. AIDED INS WITH POINT FEATURES

In this section, we briefly describe the system and measurement models of the general aided INS, which will form the basis for the ensuing analysis. In particular, the state vector of the aided INS contains the current IMU state \mathbf{x}_{IMU} and the feature ${}^G\mathbf{P}_f$ (note that for simplicity of presentation, we consider the case of a single feature):

$$\mathbf{x} = \begin{bmatrix} \mathbf{x}_{IMU}^T & {}^G\mathbf{P}_f^T \end{bmatrix}^T = \begin{bmatrix} {}^I_G\bar{q}^T & \mathbf{b}_g^T & {}^G\mathbf{V}_I^T & \mathbf{b}_a^T & {}^G\mathbf{P}_I^T & {}^G\mathbf{P}_f^T \end{bmatrix}^T \quad (1)$$

where ${}^I_G\bar{q}$ is a unit quaternion represents the rotation of IMU from the global frame to the IMU frame. ${}^G\mathbf{V}_I$ and ${}^G\mathbf{P}_I$ represents the velocity and position of the IMU in the global frame, while \mathbf{b}_g and \mathbf{b}_a represent the gyroscope and accelerometer biases, respectively.

A. IMU Propagation Model

The time evolution of the system is given by [27]:

$$\begin{aligned} {}^I_G\dot{\bar{q}}(t) &= \frac{1}{2}\Omega({}^I\omega(t)){}^I_G\bar{q}(t), & {}^G\dot{\mathbf{P}}_I(t) &= {}^G\mathbf{V}_I(t), & {}^G\dot{\mathbf{V}}_I(t) &= {}^G\mathbf{a}(t) \\ \dot{\mathbf{b}}_g(t) &= \mathbf{n}_{wg}(t), & \dot{\mathbf{b}}_a(t) &= \mathbf{n}_{wa}(t), & {}^G\dot{\mathbf{P}}_f(t) &= \mathbf{0}_{3 \times 1} \end{aligned} \quad (2)$$

where ${}^I\omega$ and ${}^I\mathbf{a}$ are the angular velocity and linear acceleration, respectively. \mathbf{n}_{wg} and \mathbf{n}_{wa} are the zero-mean Gaussian noise processes driving the gyroscope and accelerometer biases, and $\Omega(\omega) \triangleq \begin{bmatrix} -[\omega \times] & \omega \\ -\omega^\top & 0 \end{bmatrix}$, $[\omega \times]$ denotes skew symmetric matrix of ω . The gyroscope and the accelerometer measurements are:

$$\omega_m(t) = {}^I\omega(t) + \mathbf{b}_g(t) + \mathbf{n}_g(t) \quad (3)$$

$$\mathbf{a}_m(t) = \mathbf{R}({}^I_G\bar{q}(t))({}^G\mathbf{a}(t) - {}^G\mathbf{g}) + \mathbf{b}_a(t) + \mathbf{n}_a(t) \quad (4)$$

where $\mathbf{R}(\bar{q})$ represents the rotation corresponding to the quaternion \bar{q} , ${}^G\mathbf{g} = [0 \ 0 \ -g]^T$ is the gravity, $\mathbf{n}_g(t)$ and $\mathbf{n}_a(t)$ are zeros-mean Gaussian white noises corrupting angular velocity and linear acceleration measurement.

Linearizing the system model (2) at the current state estimates yields the continuous-time error-state equation [27]:

$$\dot{\tilde{\mathbf{x}}}(t) = \begin{bmatrix} \mathbf{F}_c(t) & \mathbf{0}_{15 \times 3} \\ \mathbf{0}_{3 \times 15} & \mathbf{0}_3 \end{bmatrix} \tilde{\mathbf{x}}(t) + \begin{bmatrix} \mathbf{G}(t) \\ \mathbf{0}_{3 \times 12} \end{bmatrix} \mathbf{n}(t) = \mathbf{F}(t)\tilde{\mathbf{x}}(t) + \mathbf{G}(t)\mathbf{n}(t) \quad (5)$$

where $\mathbf{F}_c(t)$ and $\mathbf{G}_c(t)$ are the continuous-time error-state transition matrix and noise Jacobian matrix. The system noise $\mathbf{n}(t) = [\mathbf{n}_g^T \ \mathbf{n}_{wg}^T \ \mathbf{n}_a^T \ \mathbf{n}_{wa}^T]^T$ are modeled as a zero-mean white Gaussian process with autocorrelation $\mathbb{E}[\mathbf{n}(t)\mathbf{n}^\top(\tau)] = \mathbf{Q}_c\delta(t-\tau)$. To propagate covariance, we need to compute the discrete-time state transition matrix $\Phi_{(k+1,k)}$ from time t_k to t_{k+1} , which is obtained by solving the differential equation $\dot{\Phi}_{(k+1,k)} = \mathbf{F}(t_k)\Phi_{(k+1,k)}$ with $\Phi_{(1,1)} =$

\mathbf{I}_{18} [1]. With that, the discrete-time noise covariance matrix and the propagated covariance can be computed as:

$$\mathbf{Q}_k = \int_{t_k}^{t_{k+1}} \Phi_{(k,\tau)} \mathbf{G}_c(\tau) \mathbf{Q}_c \mathbf{G}_c^\top(\tau) \Phi_{(k,\tau)}^\top d\tau \quad (6)$$

$$\mathbf{P}_{k+1|k} = \Phi_{(k+1,k)} \mathbf{P}_{k|k} \Phi_{(k+1,k)}^\top + \mathbf{Q}_k \quad (7)$$

B. Generic Measurement Model

A 3D point feature detected from range and/or bearing measurements, can be represented by:

$$\mathbf{P}_f = [x_f \ y_f \ z_f]^T = r_f \mathbf{b}_f \quad (8)$$

where r_f and \mathbf{b}_f are the range and bearing of the point. For simplicity, we assume the sensor frame coincides with the IMU frame. The point in the local sensor frame is given by:

$${}^I\mathbf{P}_f = [{}^Ix_f \ {}^Iy_f \ {}^Iz_f]^T = {}^I\mathbf{R}({}^G\mathbf{P}_f - {}^G\mathbf{P}_I) \quad (9)$$

While a variety of sensors are available and provide different measurements, all these measurements in the aided INS are in the form of range and/or bearing, which can be modeled generically as follows [28]:

$$\mathbf{z} = \begin{bmatrix} z^{(r)} \\ \mathbf{z}^{(b)} \end{bmatrix} = \begin{bmatrix} \sqrt{{}^I\mathbf{P}_f^\top {}^I\mathbf{P}_f} + n^{(r)} \\ \mathbf{h}_b({}^I\mathbf{P}_f, \mathbf{n}^{(b)}) \end{bmatrix} \quad (10)$$

Linearization at the current feature estimate ${}^I\hat{\mathbf{P}}_f$ yields:

$$\tilde{\mathbf{z}} = \begin{bmatrix} \tilde{z}^{(r)} \\ \tilde{\mathbf{z}}^{(b)} \end{bmatrix} \simeq \begin{bmatrix} \mathbf{H}_r {}^I\hat{\mathbf{P}}_f + n^{(r)} \\ \mathbf{H}_b {}^I\hat{\mathbf{P}}_f + \mathbf{H}_n \mathbf{n}^{(b)} \end{bmatrix} \quad (11)$$

where \mathbf{H}_r and \mathbf{H}_b denote the range and bearing measurement Jacobians, and \mathbf{H}_n is the noise Jacobian (see [28]).

III. OBSERVABILITY ANALYSIS OF AIDED INS WITH POINT FEATURES

In this section, we perform observability analysis for the linearized system of aided INS with point features based on generic measurements in a similar way as in [1], [12]. In particular, the observability matrix $\mathbf{M}(\mathbf{x})$ is given by:

$$\mathbf{M}(\mathbf{x}) = \begin{bmatrix} \mathbf{H}_{I_1} \Phi_{(1,1)} \\ \mathbf{H}_{I_2} \Phi_{(2,1)} \\ \vdots \\ \mathbf{H}_{I_k} \Phi_{(k,1)} \end{bmatrix} \quad (12)$$

The unobservable directions of this aided INS span the right null space of $\mathbf{M}(\mathbf{x})$. Specifically, for each block row of $\mathbf{M}(\mathbf{x})$, we have:

$$\mathbf{H}_{I_k} = \begin{bmatrix} \mathbf{H}_{r,k} \\ \mathbf{H}_{b,k} \end{bmatrix} = \begin{bmatrix} {}^I_G\hat{\mathbf{R}}({}^G\hat{\mathbf{P}}_f - {}^G\hat{\mathbf{P}}_{I_k}) \times \mathbf{I}_3 & \mathbf{0}_3 & \mathbf{0}_3 & \mathbf{0}_3 & -{}^I_G\hat{\mathbf{R}} & {}^I_G\hat{\mathbf{R}} \end{bmatrix} \quad (13)$$

$$= \mathbf{H}_{proj,k} {}^I_G\hat{\mathbf{R}} \begin{bmatrix} {}^G\hat{\mathbf{P}}_f - {}^G\hat{\mathbf{P}}_{I_k} \\ \mathbf{I}_3 \end{bmatrix} \times \begin{bmatrix} {}^I_G\hat{\mathbf{R}}^\top & \mathbf{0}_3 & \mathbf{0}_3 & -\mathbf{I}_3 & \mathbf{I}_3 \end{bmatrix} \quad (13)$$

where we have defined $\mathbf{H}_{proj,k} = [\mathbf{H}_{r,k}^\top \ \mathbf{H}_{b,k}^\top]^\top$. Thus,

$$\mathbf{H}_{I_k} \Phi_{(k,1)} = \mathbf{H}_{proj,k} {}^I_G\hat{\mathbf{R}} [\Gamma_1 \ \Gamma_2 \ \Gamma_3 \ \Gamma_4 \ -\mathbf{I}_3 \ \mathbf{I}_3] \quad (14)$$

where:

$$\Gamma_1 = [{}^G\hat{\mathbf{P}}_f - {}^G\hat{\mathbf{P}}_{I_1} \ - {}^G\hat{\mathbf{V}}_{I_1} \ \delta t_k \ - \frac{1}{2} {}^G\mathbf{g}(\delta t_k)^2] \times \mathbf{I}_1^\top$$

$$\Gamma_2 = [{}^G\hat{\mathbf{P}}_f - {}^G\hat{\mathbf{P}}_{I_2}] \times [{}^I_G\hat{\mathbf{R}}^\top \Phi_{12} - \Phi_{52}, \ \Gamma_3 = -\mathbf{I}_3 \delta t_k, \ \Gamma_4 = -\Phi_{54}]$$

Note that for the analysis purpose, we assume that in computing different Jacobians the linearization points for the same state variables remain the same. By inspection, it is not difficult to see that the null space for the matrix $\mathbf{M}(\mathbf{x})$ is given by:

$$\mathbf{N} = [\mathbf{N}_p \quad \mathbf{N}_r] = \begin{bmatrix} \mathbf{0}_3 & \mathbf{0}_3 & \mathbf{0}_3 & \mathbf{0}_3 & \mathbf{I}_3 & \mathbf{I}_3 \\ \left(\begin{smallmatrix} I_G \hat{\mathbf{R}}^G \mathbf{g} \end{smallmatrix} \right)^\top & \mathbf{0}_{1 \times 3} & -\left(\begin{smallmatrix} G \hat{\mathbf{V}}_{I_1} \times J^G \mathbf{g} \end{smallmatrix} \right)^\top & \mathbf{0}_{1 \times 3} & -\left(\begin{smallmatrix} G \hat{\mathbf{P}}_{I_1} \times J^G \mathbf{g} \end{smallmatrix} \right)^\top & -\left(\begin{smallmatrix} G \hat{\mathbf{P}}_{I_2} \times J^G \mathbf{g} \end{smallmatrix} \right)^\top \end{bmatrix}^\top \quad (15)$$

where \mathbf{N}_p corresponds to the sensor's global translation and \mathbf{N}_r relates to the global rotation around the gravity direction. For generic range and bearing sensors, the measurement Jacobian w.r.t. $I_k \mathbf{P}_f$ can all be represented by $\mathbf{H}_{proj,k}$. From the above analysis, we see that the system has at least four unobservable directions.

Additionally, in analogy to [2], [12], [21], we have further performed the nonlinear observability analysis based on lie derivatives [20] for the continuous-time nonlinear INS aided by generic measurements, which is summarized as follows:

Lemma 1. *The continuous-time nonlinear INS aided by generic range and/or bearing measurements with point features, has 4 unobservable directions.*

Proof. See [28]. \square

A. Global Measurements

In practice, the aided INS may also have access to (partial) global measurements provided by, for example, GPS, motion capture systems, barometers and compasses. Intuitively, such measurements would alter the system observability properties, even if only partial (not full 6DOF) information is available. In what follows, we systematically inspect the impacts of such measurements on observability.

1) *Global Position Measurements:* We consider the case where besides the range and bearing sensors, global position measurements are also available from, for example, GPS and barometer. Specifically, if sensor's translation along x direction is known, the additional measurement is given by $z^{(x)} = \mathbf{e}_1^\top G \mathbf{P}_I$. The measurement Jacobians and the block row of observability matrix at time step k can be computed as:

$$\begin{aligned} \mathbf{H}_{I_k} &= \begin{bmatrix} \mathbf{H}_{r,k} \\ \mathbf{H}_{b,k} \\ \mathbf{H}_{x,k} \end{bmatrix} = \begin{bmatrix} \mathbf{H}_{proj,k} I_G \hat{\mathbf{R}} \left[\left(\begin{smallmatrix} G \hat{\mathbf{P}}_f - G \hat{\mathbf{P}}_{I_k} \end{smallmatrix} \right) \times J^G \hat{\mathbf{R}}^\top \quad \mathbf{0}_3 \quad \mathbf{0}_3 \quad \mathbf{0}_3 \quad -\mathbf{I}_3 \quad \mathbf{I}_3 \right] \\ \mathbf{0}_{1 \times 3} \quad \mathbf{0}_{1 \times 3} \quad \mathbf{0}_{1 \times 3} \quad \mathbf{0}_{1 \times 3} \quad \mathbf{e}_1^\top \quad \mathbf{0}_{1 \times 3} \end{bmatrix} \\ &\Rightarrow \mathbf{H}_k \Phi_{(k,1)} = \begin{bmatrix} \mathbf{H}_{proj,k} I_G \hat{\mathbf{R}} \left[\Gamma_1 \quad \Gamma_2 \quad \Gamma_3 \quad \Gamma_4 \quad -\mathbf{I}_3 \quad \mathbf{I}_3 \right] \\ \mathbf{0}_{1 \times 3} \quad \mathbf{0}_{1 \times 3} \quad \mathbf{0}_{1 \times 3} \quad \mathbf{0}_{1 \times 3} \quad \mathbf{e}_1^\top \quad \mathbf{0}_{1 \times 3} \end{bmatrix} \end{aligned} \quad (16)$$

where $\mathbf{H}_{x,k}$ is the measurement Jacobians for global x measurement. We can show that the system's unobservable directions now become:

$$\mathbf{N}_x = \begin{bmatrix} \mathbf{0}_{2 \times 3} & \mathbf{0}_{2 \times 3} & \mathbf{0}_{2 \times 3} & \mathbf{0}_{2 \times 3} & [\mathbf{0}_{2 \times 1} \quad \mathbf{I}_2] & [\mathbf{0}_{2 \times 1} \quad \mathbf{I}_2] \end{bmatrix}^\top \quad (17)$$

Compared to \mathbf{N} in (15), both sensor's global translation in x direction and the rotation around the gravity direction become observable. Analogously, if global y -axis measurement is available, translation along y and rotation around gravity direction will become observable [28].

Proceeding similarly, if the sensor's translation in z direction is directly measured, e.g., by a barometer, we have an additional measurement $z^{(z)} = \mathbf{e}_3^\top G \mathbf{P}_I$. In this case, the block row of the observability matrix at time step k becomes:

$$\mathbf{H}_k \Phi_{(k,1)} = \begin{bmatrix} \mathbf{H}_{proj,k} I_G \hat{\mathbf{R}} \left[\Gamma_1 \quad \Gamma_2 \quad \Gamma_3 \quad \Gamma_4 \quad -\mathbf{I}_3 \quad \mathbf{I}_3 \right] \\ \mathbf{0}_{1 \times 3} \quad \mathbf{0}_{1 \times 3} \quad \mathbf{0}_{1 \times 3} \quad \mathbf{0}_{1 \times 3} \quad \mathbf{e}_3^\top \quad \mathbf{0}_{1 \times 3} \end{bmatrix} \quad (18)$$

Since \mathbf{e}_3 is parallel to $G \mathbf{g}$, then $\mathbf{e}_3^\top [G \mathbf{P}_I \times J^G \mathbf{g}] = 0$. Therefore, the system's unobservable directions become \mathbf{N}_z :

$$\mathbf{N}_z^\top = \begin{bmatrix} \mathbf{0}_{2 \times 3} & \mathbf{0}_{2 \times 3} & \mathbf{0}_{2 \times 3} & \mathbf{0}_{2 \times 3} & [\mathbf{I}_2 \quad \mathbf{0}_{1 \times 2}] & [\mathbf{I}_2 \quad \mathbf{0}_{1 \times 2}]^\top \\ \left(\begin{smallmatrix} I_G \hat{\mathbf{R}}^G \mathbf{g} \end{smallmatrix} \right)^\top & \mathbf{0}_{1 \times 3} & -\left(\begin{smallmatrix} G \hat{\mathbf{V}}_{I_1} \times J^G \mathbf{g} \end{smallmatrix} \right)^\top & \mathbf{0}_{1 \times 3} & -\left(\begin{smallmatrix} G \hat{\mathbf{P}}_{I_1} \times J^G \mathbf{g} \end{smallmatrix} \right)^\top & -\left(\begin{smallmatrix} G \hat{\mathbf{P}}_{I_2} \times J^G \mathbf{g} \end{smallmatrix} \right)^\top \end{bmatrix}$$

Clearly, only translation in z becomes observable, while, different from the cases with global x and y measurements, the rotation around gravity direction is still unobservable.

2) *Global Orientation Measurements:* If the aided INS is equipped with a magnetic compass, then we also have global orientation measurements given by $z^{(N)} = I_N \mathbf{n} = I_G \mathbf{R}^G \mathbf{n}_n$. In this case, the Jacobians and the block row of the observability matrix at time step k can be computed as:

$$\begin{aligned} \mathbf{H}_{I_k} &= \begin{bmatrix} \mathbf{H}_{r,k} \\ \mathbf{H}_{b,k} \\ \mathbf{H}_{N,k} \end{bmatrix} = \begin{bmatrix} \mathbf{H}_{proj,k} I_G \hat{\mathbf{R}} \left[\left(\begin{smallmatrix} G \hat{\mathbf{P}}_f - G \hat{\mathbf{P}}_{I_k} \end{smallmatrix} \right) \times J^G \hat{\mathbf{R}}^\top \quad \mathbf{0}_3 \quad \mathbf{0}_3 \quad \mathbf{0}_3 \quad -\mathbf{I}_3 \quad \mathbf{I}_3 \right] \\ I_G \hat{\mathbf{R}} \left[\left(\begin{smallmatrix} G \mathbf{n}_n \times I_G \hat{\mathbf{R}}^\top \end{smallmatrix} \right) \mathbf{0}_3 \quad \mathbf{0}_3 \quad \mathbf{0}_3 \quad \mathbf{0}_3 \quad \mathbf{0}_3 \right] \\ \mathbf{0}_{1 \times 3} \end{bmatrix} \\ &\Rightarrow \mathbf{H}_k \Phi_{(k,1)} = \begin{bmatrix} \mathbf{H}_{proj,k} I_G \hat{\mathbf{R}} \left[\Gamma_1 \quad \Gamma_2 \quad \Gamma_3 \quad \Gamma_4 \quad -\mathbf{I}_3 \quad \mathbf{I}_3 \right] \\ I_G \hat{\mathbf{R}} \left[\left(\begin{smallmatrix} G \mathbf{n}_n \times I_I \hat{\mathbf{R}}^\top \end{smallmatrix} \right) \Gamma_5 \quad \mathbf{0}_3 \quad \mathbf{0}_3 \quad \mathbf{0}_3 \quad \mathbf{0}_3 \right] \end{bmatrix} \end{aligned} \quad (19)$$

where $\mathbf{H}_{N,k}$ is the Jacobians for orientation measurement, and $\Gamma_5 = [G \mathbf{n}_n \times I_I \hat{\mathbf{R}}^\top] \mathbf{P}_{I_2}$. If $G \mathbf{n}_n$ is not parallel to $G \mathbf{g}$, $[G \mathbf{N}_n \times G \mathbf{g}] \neq 0$, the rotation around the gravity direction becomes observable, and the unobservable directions become:

$$\mathbf{N}_n = [\mathbf{0}_3 \quad \mathbf{0}_3 \quad \mathbf{0}_3 \quad \mathbf{0}_3 \quad \mathbf{I}_3 \quad \mathbf{I}_3]^\top \quad (20)$$

In summary, as expected, global measurements will make the system more observable. If a global full position measurements by GPS or a prior map are available, the system will become fully observable, while global orientation measurements can make the rotation around gravitational direction observable, as long as this orientation is not parallel to the direction of gravity.

B. Degenerate Motion

We further investigate degenerate motion for INS aided with generic range and bearing sensors, which is important for healthy estimators. As compared to [22] where pure translation or constant acceleration have been reported to be degenerate in VINS, we identify 2 more degenerate cases: pure rotation and translation towards a feature. To ease the analysis, we use range and bearing parameterization (i.e., spherical coordinates) of the point feature, instead of the conventional 3D Euclidean coordinates.

$$\mathbf{P}_f = \begin{bmatrix} x_f \\ y_f \\ z_f \end{bmatrix} = r_f \mathbf{b}_f = r_f \begin{bmatrix} \cos \theta \cos \phi \\ \sin \theta \cos \phi \\ \sin \phi \end{bmatrix} \quad (21)$$

where r_f is the range, θ and ϕ represents the horizontal and elevation angle of point feature. With that, the state becomes:

$$\mathbf{x} = \begin{bmatrix} I_G \bar{q}^\top & \mathbf{b}_g^\top & G \mathbf{V}_I^\top & \mathbf{b}_a^\top & G \mathbf{P}_I^\top & [G_r \quad G_\theta \quad G_\phi]^\top \end{bmatrix}^\top \quad (22)$$

In this case, we can write the block row of the observability matrix as:

$$\begin{aligned} \mathbf{H}_k &= \mathbf{H}_{proj,k}{}^I_G \hat{\mathbf{R}} \left[\left({}^G \hat{\mathbf{P}}_f - {}^G \hat{\mathbf{P}}_k \right) \times \right] {}^I_G \hat{\mathbf{R}}^\top \quad \mathbf{0}_3 \quad \mathbf{0}_3 \quad \mathbf{0}_3 \quad -\mathbf{I}_3 \quad \begin{bmatrix} \frac{\partial {}^G \hat{\mathbf{P}}_k}{\partial {}^G \hat{r}_f} & \frac{\partial {}^G \hat{\mathbf{P}}_k}{\partial {}^G \theta_f} & \frac{\partial {}^G \hat{\mathbf{P}}_k}{\partial {}^G \phi_f} \end{bmatrix} \\ \Rightarrow \mathbf{H}_k \Phi_{(k,1)} &= \mathbf{H}_{b,k} {}^I_G \hat{\mathbf{R}} \begin{bmatrix} \Gamma_1 & \Gamma_2 & \Gamma_3 & \Gamma_4 & -\mathbf{I}_3 & \hat{\mathbf{b}}_f & {}^G \hat{r}_f \cos \phi \hat{\mathbf{b}}_1^\perp & {}^G \hat{r}_f \hat{\mathbf{b}}_2^\perp \end{bmatrix} \end{aligned} \quad (23)$$

where

$$\begin{aligned} \frac{\partial {}^G \hat{\mathbf{P}}_f}{\partial {}^G \hat{r}_f} &= \begin{bmatrix} \cos \hat{\theta} \cos \hat{\phi} & \sin \hat{\theta} \cos \hat{\phi} & \sin \hat{\phi} \end{bmatrix}^\top \triangleq \hat{\mathbf{b}}_f \\ \frac{\partial {}^G \hat{\mathbf{P}}_f}{\partial {}^G \theta_f} &= \begin{bmatrix} -\sin \hat{\theta} & \cos \hat{\theta} & 0 \end{bmatrix}^\top {}^G \hat{r}_f \cos \hat{\phi} \triangleq {}^G \hat{r}_f \cos \hat{\phi} \hat{\mathbf{b}}_1^\perp \\ \frac{\partial {}^G \hat{\mathbf{P}}_f}{\partial {}^G \phi_f} &= \begin{bmatrix} -\cos \hat{\theta} \sin \hat{\phi} & -\sin \hat{\theta} \sin \hat{\phi} & \cos \hat{\phi} \end{bmatrix}^\top {}^G \hat{r}_f \triangleq {}^G \hat{r}_f \hat{\mathbf{b}}_2^\perp \end{aligned}$$

By inspection, the unobservable directions are given by:

$$\begin{aligned} \mathbf{N}_{rb} &= [\mathbf{N}_{rb,p} \quad \mathbf{N}_{rb,r}] = \\ &\begin{bmatrix} \mathbf{0}_3 & \mathbf{0}_3 & \mathbf{0}_3 & \mathbf{0}_3 & \mathbf{I}_3 & \hat{\mathbf{b}}_f & \frac{1}{{}^G \hat{r}_f \cos \phi} \hat{\mathbf{b}}_1^\perp & \frac{1}{{}^G \hat{r}_f} \hat{\mathbf{b}}_2^\perp \\ \left({}^I_G \hat{\mathbf{R}} {}^G \mathbf{g} \right)^\top & \mathbf{0}_{1 \times 3} & -\left([{}^G \hat{\mathbf{V}}_I \times] {}^G \mathbf{g} \right)^\top & \mathbf{0}_{1 \times 3} & -\left([{}^G \hat{\mathbf{P}}_I \times] {}^G \mathbf{g} \right)^\top & 0 & -g & 0 \end{bmatrix}^\top \end{aligned} \quad (24)$$

where $g = \| {}^G \mathbf{g} \|$, $\mathbf{N}_{rb,p}$ and $\mathbf{N}_{rb,r}$ denote the unobservable directions related to the global translation and global rotation around the gravity direction, which as expected agrees with the preceding analysis.

1) *Pure Translation*: If the sensor undergoes pure translation, the system gain additional unobservable directions:

$$\mathbf{N}_R = \begin{bmatrix} {}^I_G \hat{\mathbf{R}}^\top & \mathbf{0}_3 & -\left([{}^G \hat{\mathbf{V}}_I \times] \right)^\top & \left({}^I_G \hat{\mathbf{R}} [{}^G \mathbf{g} \times] \right)^\top & -\left([{}^G \hat{\mathbf{P}}_I \times] \right)^\top & -\Theta^\top \end{bmatrix} \quad (25)$$

where $\Theta = \begin{bmatrix} 0 & 0 & 0 \\ {}^G \hat{r}_f \cos \hat{\theta} \tan \hat{\phi} & \sin \hat{\theta} \tan \hat{\phi} & -1 \\ -{}^G \hat{r}_f \sin \hat{\theta} & \cos \hat{\theta} & 0 \end{bmatrix}$. Similar to [22], this unobservable direction can be easily verified as follows:

$$\mathbf{H}_k \Phi(k,1) \mathbf{N}_R = \mathbf{H}_{proj,k} {}^I_G \hat{\mathbf{R}} \left(\Gamma_4 {}^I_G \hat{\mathbf{R}} - \frac{1}{2} \delta t_k^2 \mathbf{I}_3 \right) [{}^G \mathbf{g} \times] = \mathbf{0} \quad (26)$$

From Θ we see that this unobservable direction only relates to the bearing of the feature, since the first row of Θ are all zeros. This indicates that the global rotation of the sensor all becomes unobservable, rather than only global yaw unobservable for general motion. It is important to note that no assumption is made about sensors used in this analysis.

2) *Pure Rotation*: If sensor has only rotational motion, then ${}^G \hat{\mathbf{P}}_k = \mathbf{0}_{3 \times 1}$ and we have ${}^I_k \mathbf{P}_f = {}^I_G \hat{\mathbf{R}} {}^G \mathbf{P}_f$. For mono-camera, the system will gain one more unobservable direction corresponding to the feature's range:

$$\mathbf{N}_1 = [\mathbf{0}_{1 \times 3} \quad \mathbf{0}_{1 \times 3} \quad \mathbf{0}_{1 \times 3} \quad \mathbf{0}_{1 \times 3} \quad \mathbf{0}_{1 \times 3} \quad 1 \quad 0 \quad 0]^\top \quad (27)$$

Since a mono-camera provides only bearing measurements, $\mathbf{H}_{proj,k} = \mathbf{H}_{b,k}$ (see [28]). In this case, we have:

$$\mathbf{H}_k \Phi_{(k,1)} \mathbf{N}_1 = \mathbf{H}_{b,k} {}^I \hat{\mathbf{b}}_f = \mathbf{H}_{b,k} {}^I_G \hat{\mathbf{R}} {}^G \hat{\mathbf{b}}_f = \mathbf{0}$$

Therefore, we have one more unobservable direction related to the scale of the feature.

3) *Moving Toward a Feature*: If the mono-camera is moving towards a feature, then the system will also gain one more unobservable direction related to this feature scale:

$$\mathbf{N}_1 = [\mathbf{0}_{1 \times 3} \quad \mathbf{0}_{1 \times 3} \quad \mathbf{0}_{1 \times 3} \quad \mathbf{0}_{1 \times 3} \quad \mathbf{0}_{1 \times 3} \quad 1 \quad 0 \quad 0]^\top \quad (28)$$

This degenerate motion indicates that the sensor is moving along the direction of the feature's bearing direction, that

is: ${}^G \mathbf{P}_{I_k} = \alpha {}^G \mathbf{b}_f$, with α denotes the scale of the sensor's motion. Then, we can arrive at:

$${}^I_k \mathbf{P}_f = {}^I_k r_f {}^I_k \mathbf{b}_f = {}^I_G \mathbf{R} \left({}^G \mathbf{P}_f - {}^G \mathbf{P}_{I_k} \right) = {}^I_G \mathbf{R} \left({}^G r_f - \alpha \right) {}^G \mathbf{b}_f \quad (29)$$

Similar to the case of pure rotation, we can show the additional unobservable direction \mathbf{N}_1 based on the following:

$$\mathbf{H}_{b,k} \Phi_{(k,1)} \mathbf{N}_1 = \frac{{}^I \hat{r}_f}{{}^I \hat{r}_f - \alpha} \mathbf{H}_{b,k} {}^I_G \hat{\mathbf{R}} {}^G \hat{\mathbf{b}}_f = \mathbf{0}_{2 \times 1}$$

4) *Constant Acceleration*: If the mono-camera moves with constant local acceleration, i.e., ${}^I_k \mathbf{a}$ is constant, then the system will have one more unobservable direction given by:

$$\mathbf{N}_a = [\mathbf{0}_{1 \times 3} \quad \mathbf{0}_{1 \times 3} \quad {}^G \hat{\mathbf{V}}_I^\top \quad -{}^I \hat{\mathbf{a}}^\top \quad {}^G \hat{\mathbf{P}}_I^\top \quad {}^G \hat{r}_f \quad 0 \quad 0]^\top \quad (30)$$

To see this, we have:

$$\mathbf{H}_k \Phi_{(k,1)} \mathbf{N}_a = \mathbf{H}_{b,k} {}^I_G \hat{\mathbf{R}} \left(-{}^G \hat{\mathbf{V}}_I \delta t_k - \Gamma_4 {}^I \hat{\mathbf{a}} - {}^G \hat{\mathbf{P}}_I \delta t_k + {}^G r_f {}^G \hat{\mathbf{b}}_f \right) \quad (31)$$

Based on [22], we know:

$$\Gamma_4 {}^I \mathbf{a} = {}^G \hat{\mathbf{P}}_I - {}^G \hat{\mathbf{P}}_I - {}^G \hat{\mathbf{V}}_I \delta t_k \quad (32)$$

Therefore, we arrive at:

$$\mathbf{H}_k \Phi_{(k,1)} \mathbf{N}_a = \mathbf{H}_{b,k} {}^I_G \hat{\mathbf{R}} \left({}^G \hat{\mathbf{P}}_I - {}^G \hat{\mathbf{P}}_I \right) = \mathbf{H}_{b,k} {}^I \hat{\mathbf{P}}_f = \mathbf{0}_{2 \times 1} \quad (33)$$

Clearly, this null space is only related to the scale; thus, if we use sensors such as stereo and RGBD cameras that can recover the scale, this unobservable direction will disappear.

IV. OBSERVABILITY ANALYSIS OF AIDED INS WITH LINE FEATURES

As navigating in structured environments, line features can be used in the aided INS to provide more compact information. Thus, in this section, we perform observability analysis for the aided INS with line features to provide insights for building consistent estimators.

A. Line Representation

Inspired by [26], we propose to use the Plücker representation for the line feature in the state vector while *orthonormal representation* (which is minimal) for the error state. The Plücker representation can be initialized by the two end points \mathbf{P}_{L_1} and \mathbf{P}_{L_2} of a line segment L , as:

$$\mathbf{L} = \begin{bmatrix} [\mathbf{P}_{L_1} \times] \mathbf{P}_{L_2} \\ \mathbf{P}_{L_2} - \mathbf{P}_{L_1} \end{bmatrix} = \begin{bmatrix} \mathbf{n}_L \\ \mathbf{v}_L \end{bmatrix} \quad (34)$$

where \mathbf{n}_L and \mathbf{v}_L are the normal vector and direction vector for the line \mathbf{L} . We need a minimal parameterization for line error states. Based on (34), we have:

$$\mathbf{L} = [\mathbf{n}_L | \mathbf{v}_L] = \begin{bmatrix} \frac{\mathbf{n}_L}{\|\mathbf{n}_L\|} & \frac{\mathbf{v}_L}{\|\mathbf{v}_L\|} & \frac{\mathbf{n}_L \times \mathbf{v}_L}{\|\mathbf{n}_L \times \mathbf{v}_L\|} \end{bmatrix} \begin{bmatrix} \|\mathbf{n}_L\| & 0 \\ 0 & \|\mathbf{v}_L\| \\ 0 & 0 \end{bmatrix} \quad (35)$$

where we can define:

$$\begin{aligned} \mathbf{R}_L(\theta_L) &= \exp(-[\theta_L \times]) = \begin{bmatrix} \frac{\mathbf{n}_L}{\|\mathbf{n}_L\|} & \frac{\mathbf{v}_L}{\|\mathbf{v}_L\|} & \frac{\mathbf{n}_L \times \mathbf{v}_L}{\|\mathbf{n}_L \times \mathbf{v}_L\|} \end{bmatrix} \\ \mathbf{W}_L(\phi_L) &= \frac{1}{\sqrt{w_1^2 + w_2^2}} \begin{bmatrix} w_1 & -w_2 \\ w_2 & w_1 \end{bmatrix} = \eta \begin{bmatrix} \|\mathbf{n}_L\| & -\|\mathbf{v}_L\| \\ \|\mathbf{v}_L\| & \|\mathbf{n}_L\| \end{bmatrix} \end{aligned}$$

where $w_1 = \|\mathbf{n}_L\|$, $w_2 = \|\mathbf{v}_L\|$ and $\eta = \frac{1}{\sqrt{w_1^2 + w_2^2}}$. Since $\mathbf{R}_L \in \mathbf{SO}(3)$ and $\mathbf{W}_L \in \mathbf{SO}(2)$, we can define the error states

for these parameters as $\delta\theta_L$ and $\delta\phi_L$ (from \mathbf{R}_L and \mathbf{W}_L), respectively. With that, the state can be written as:

$$\mathbf{x} = \begin{bmatrix} {}^I_G\hat{\mathbf{q}}^\top & \mathbf{b}_g^\top & {}^G\mathbf{V}_I^\top & \mathbf{b}_a^\top & {}^G\mathbf{P}_I^\top & {}^G\mathbf{L}_f^\top \end{bmatrix}^\top$$

where ${}^G\mathbf{L}_f = [{}^G\mathbf{n}_L^\top \ {}^G\mathbf{v}_L^\top]^\top$ and ${}^G\tilde{\mathbf{L}}_f = [\delta\theta_L^\top \ \delta\phi_L^\top]^\top$.

B. Observability Analysis: Single Line

Without loss of generality, consider stereo images are available for detecting and tracking line features. Measurements for the line are given by the distance of the two end points \mathbf{x}_s and \mathbf{x}_e to the line [29]:

$$\mathbf{z} = \begin{bmatrix} \frac{\mathbf{x}_s^\top \mathbf{l}'}{\sqrt{l_1^2 + l_2^2}} & \frac{\mathbf{x}_e^\top \mathbf{l}'}{\sqrt{l_1^2 + l_2^2}} \end{bmatrix}^\top \quad (36)$$

where we have used:

$$\mathbf{l}' = \begin{bmatrix} f_1 & 0 & 0 \\ 0 & f_2 & 0 \\ -f_2 c_1 & f_1 c_2 & f_1 f_2 \end{bmatrix}, {}^I\mathbf{n}_L = \begin{bmatrix} l_1 \\ l_2 \\ l_3 \end{bmatrix}, {}^I\mathbf{L} = \begin{bmatrix} {}^I_G\mathbf{R} & -{}^I_G\mathbf{R}[{}^G\mathbf{P}_I \times] \\ \mathbf{0}_3 & {}^I_G\mathbf{R} \end{bmatrix} {}^G\mathbf{L}$$

Note that f_1 , f_2 , c_1 and c_2 are camera intrinsic parameters. With the line measurements, we compute line measurement Jacobians and the block row of the observability matrix at time step k as follows:

$$\frac{\partial \tilde{\mathbf{z}}}{\partial \tilde{\mathbf{y}}} = \frac{\partial \tilde{\mathbf{z}}}{\partial \tilde{\mathbf{l}'}} \mathbf{K}_G^I \hat{\mathbf{R}} \left[\left({}^G\hat{\mathbf{n}}_L \times \right) - \left({}^G\hat{\mathbf{P}}_I \times \right) {}^G\hat{\mathbf{v}}_L \times \right] {}^I_G\hat{\mathbf{R}}^\top \ \mathbf{0}_{3 \times 9} \ [{}^G\hat{\mathbf{v}}_L \times] \ \Gamma_{14} \ \Gamma_{15}$$

$$\mathbf{H}_k \Phi(k, 1) = \frac{\partial \tilde{\mathbf{z}}}{\partial \tilde{\mathbf{l}'}} \mathbf{K}_G^I \hat{\mathbf{R}} \left[\Gamma_{11} \ \Gamma_{12} \ [{}^G\hat{\mathbf{v}}_L \times] \delta t_k \ \Gamma_{13} \ [{}^G\hat{\mathbf{v}}_L \times] \ \Gamma_{14} \ \Gamma_{15} \right]$$

where $\Gamma_{li}, i \in \{1 \dots 5\}$ are derived in our technical report [28]. We also define $e_1 = \mathbf{x}_s^\top \mathbf{l}'$, $e_2 = \mathbf{x}_e^\top \mathbf{l}'$, $l_n = \sqrt{(l_1^2 + l_2^2)}$, $\mathbf{x}_s = [u_1, v_1, 1]^\top$ and $\mathbf{x}_e = [u_2, v_2, 1]^\top$. With these, we have:

$$\frac{\partial \tilde{\mathbf{z}}}{\partial \tilde{\mathbf{l}'}} = \frac{1}{l_n} \begin{bmatrix} u_1 - \frac{l_1 e_1}{l_n^2} & v_1 - \frac{l_2 e_1}{l_n^2} & 1 \\ u_2 - \frac{l_1 e_2}{l_n^2} & v_2 - \frac{l_2 e_2}{l_n^2} & 1 \end{bmatrix} \quad (37)$$

It can be shown that the linearized aided INS system with a line feature will have at least 5 unobservable directions [28]:

$$\mathbf{N}_l = [\mathbf{N}_{l1} \ \mathbf{N}_{l2} \ \mathbf{N}_{l3} \ \mathbf{N}_{l4} \ \mathbf{N}_{l5}] \quad (38)$$

$$= \begin{bmatrix} {}^I_G\hat{\mathbf{R}}^G \mathbf{g} & \mathbf{0}_{3 \times 1} & \mathbf{0}_{3 \times 1} & \mathbf{0}_{3 \times 1} & \mathbf{0}_{3 \times 1} \\ \mathbf{0}_{3 \times 1} & \mathbf{0}_{3 \times 1} & \mathbf{0}_{3 \times 1} & \mathbf{0}_{3 \times 1} & \mathbf{0}_{3 \times 1} \\ -[{}^G\hat{\mathbf{V}}_I \times] {}^G\mathbf{g} & \mathbf{0}_{3 \times 1} & \mathbf{0}_{3 \times 1} & \mathbf{0}_{3 \times 1} & {}^G\hat{\mathbf{v}}_e \\ \mathbf{0}_{3 \times 1} & \mathbf{0}_{3 \times 1} & \mathbf{0}_{3 \times 1} & \mathbf{0}_{3 \times 1} & \mathbf{0}_{3 \times 1} \\ -[{}^G\hat{\mathbf{P}}_I \times] {}^G\mathbf{g} & \mathbf{0}_{3 \times 1} & {}^G\hat{\mathbf{v}}_e & [{}^G\hat{\mathbf{n}}_L \times] {}^G\hat{\mathbf{v}}_e & \mathbf{0}_{3 \times 1} \\ -{}^G\mathbf{g} & \frac{w_2 G \hat{\mathbf{v}}_e}{w_1} & \mathbf{0}_{3 \times 1} & \mathbf{0}_{3 \times 1} & \mathbf{0}_{3 \times 1} \\ 0 & 0 & 0 & \eta^2 w_2^2 & 0 \end{bmatrix}$$

where ${}^G\hat{\mathbf{n}}_e$ and ${}^G\hat{\mathbf{v}}_e$ is the unit direction for ${}^G\hat{\mathbf{n}}_L$ and ${}^G\hat{\mathbf{v}}_L$, respectively. Note that \mathbf{N}_{l1} relates to the rotation around the gravitational direction, $\mathbf{N}_{l2:4}$ relates to the sensor's global translation, while \mathbf{N}_{l5} relates to the sensor motion along the line direction.

C. Observability Analysis: Multiple Lines

Assuming there are $m > 1$ un-parallel lines in the state vector, we define the orientation ${}^G_L\mathbf{R}$ of a line i and the rotation ${}^{L_i}\mathbf{R}$ between line i and line j ($i, j \in \{1, \dots, m\}$) as:

$${}^{L_i}\hat{\mathbf{R}} = \begin{bmatrix} {}^G\hat{\mathbf{n}}_{ei} & {}^G\hat{\mathbf{v}}_{ei} & [{}^G\hat{\mathbf{n}}_{ei} \times] {}^G\hat{\mathbf{v}}_{ei} \end{bmatrix} \quad (39)$$

$${}^{L_j}\hat{\mathbf{R}} = {}^{L_i}\hat{\mathbf{R}} {}^{G_L}\hat{\mathbf{R}} \quad (40)$$

Lemma 2. For the aided INS with $m > 1$ un-parallel line features in the state vector, the system will have at least 4 unobservable directions.

Proof. See [28]. \square

V. OBSERVABILITY ANALYSIS OF AIDED INS WITH PLANE FEATURES

In analogy to the case of line features, in this section we extend the observability analysis to the aided INS with plane features. In particular, for any point \mathbf{P}_f in a plane Π , we have $\mathbf{n}_\Pi^\top \mathbf{P}_f + d = 0$, where \mathbf{n}_Π is the normal direction of this plane and $|d|$ is the distance from the origin to plane Π . Hence, plane Π can be represented as:

$$\Pi = \begin{bmatrix} \mathbf{n}_\Pi^\top & d \end{bmatrix}^\top \quad (41)$$

We still need a minimal error state representation for plane update. Notice that a horizontal angle θ and elevation angle ϕ can be used to describe the normal direction \mathbf{n}_Π as:

$$\mathbf{n}_\Pi = \begin{bmatrix} n_1 \\ n_2 \\ n_3 \end{bmatrix} = \begin{bmatrix} \cos \theta \cos \phi \\ \sin \theta \cos \phi \\ \sin \phi \end{bmatrix} \quad (42)$$

Thus, the error state for the plane can be denoted as $\tilde{\Pi} = [\tilde{\theta} \ \tilde{\phi} \ d]^\top$. Accordingly, the state vector of the system with one plane feature becomes:

$$\mathbf{x} = \begin{bmatrix} {}^I_G\hat{\mathbf{q}}^\top & \mathbf{b}_g^\top & {}^G\mathbf{V}_I^\top & \mathbf{b}_a^\top & {}^G\mathbf{P}_I^\top & {}^G\Pi^\top \end{bmatrix}^\top \quad (43)$$

A. Observability Analysis: Single Plane

Plane features can be extracted from point cloud (of RGBD, stereo cameras or 3D LiDAR). Hence, we assume a direct plane measurement given by:

$$\mathbf{z} = \begin{bmatrix} {}^I\theta & {}^I\phi & {}^I d \end{bmatrix}^\top \quad (44)$$

The measurement Jacobian w.r.t. ${}^I\mathbf{n}_\Pi$ and ${}^I d$ can be computed as follows:

$$\mathbf{H}_\Pi = \begin{bmatrix} -\frac{\hat{n}_2}{\hat{n}_1^2 + \hat{n}_2^2} & \frac{\hat{n}_1}{\hat{n}_1^2 + \hat{n}_2^2} & 0 & 0 \\ -\frac{\hat{n}_1 \hat{n}_3}{\sqrt{\hat{n}_1^2 + \hat{n}_2^2}} & -\frac{\hat{n}_2 \hat{n}_3}{\sqrt{\hat{n}_1^2 + \hat{n}_2^2}} & \sqrt{\hat{n}_1^2 + \hat{n}_2^2} & 0 \\ 0 & 0 & 0 & 1 \end{bmatrix} \quad (45)$$

Hence, we get the measurement Jacobians w.r.t. the \mathbf{x} as:

$$\begin{aligned} \frac{\partial \tilde{\mathbf{z}}}{\partial \tilde{\mathbf{x}}} &= \mathbf{H}_\Pi \begin{bmatrix} [{}^I_G\hat{\mathbf{R}}^G \hat{\mathbf{n}} \times] & \mathbf{0}_3 & \mathbf{0}_3 & \mathbf{0}_3 & {}^I_G\hat{\mathbf{R}}^G \hat{\mathbf{n}}_1^\perp \cos \hat{\phi} & {}^I_G\hat{\mathbf{R}}^G \hat{\mathbf{n}}_2^\perp & \mathbf{0}_{3 \times 1} \\ \mathbf{0}_{1 \times 3} & \mathbf{0}_{1 \times 3} & \mathbf{0}_{1 \times 3} & \mathbf{0}_{1 \times 3} & {}^I_G\mathbf{P}_I^\top {}^I_G\hat{\mathbf{n}}_1^\perp \cos \hat{\phi} & {}^I_G\mathbf{P}_I^\top {}^I_G\hat{\mathbf{n}}_2^\perp & 1 \end{bmatrix} \\ \Rightarrow \mathbf{H}_k \Phi(k, 1) &= \mathbf{H}_\Pi \begin{bmatrix} \Gamma_{\Pi 1} & \Gamma_{\Pi 2} & \begin{bmatrix} \mathbf{0}_3 \\ {}^G\hat{\mathbf{n}}^\top \delta t_k \end{bmatrix} & \Gamma_{\Pi 3} & \begin{bmatrix} \mathbf{0}_3 \\ {}^G\hat{\mathbf{n}}^\top \end{bmatrix} & \Gamma_{\Pi 4} \end{bmatrix} \end{aligned}$$

where:

$$\begin{aligned} \Gamma_{\Pi 1} &= \begin{bmatrix} {}^I_G\hat{\mathbf{R}}[{}^G\hat{\mathbf{n}} \times] \\ {}^G\mathbf{n}^\top [({}^G\hat{\mathbf{P}}_I + {}^G\hat{\mathbf{V}}_I \delta t_k - \frac{1}{2} {}^G\mathbf{g} \delta t_k^2 - {}^G\hat{\mathbf{P}}_k) \times] \end{bmatrix} {}^I_G\hat{\mathbf{R}} \\ \Gamma_{\Pi 2} &= \begin{bmatrix} {}^I_G\hat{\mathbf{R}}[{}^G\hat{\mathbf{n}} \times] {}^I_G\hat{\mathbf{R}}^\top \Phi_{12} \\ {}^G\hat{\mathbf{n}}^\top \Phi_{52} \end{bmatrix}, \quad \Gamma_{\Pi 3} = \begin{bmatrix} \mathbf{0}_3 \\ {}^G\hat{\mathbf{n}}^\top \Phi_{54} \end{bmatrix} \\ \Gamma_{\Pi 4} &= \begin{bmatrix} {}^I_G\hat{\mathbf{R}}^G \hat{\mathbf{n}}_1^\perp \cos \hat{\phi} & {}^I_G\hat{\mathbf{R}}^G \hat{\mathbf{n}}_2^\perp & \mathbf{0}_{3 \times 1} \\ {}^I_G\mathbf{P}_I^\top {}^I_G\hat{\mathbf{n}}_1^\perp \cos \hat{\phi} & {}^I_G\mathbf{P}_I^\top {}^I_G\hat{\mathbf{n}}_2^\perp & 1 \end{bmatrix} \\ {}^G\mathbf{n}_1^\perp &= \begin{bmatrix} -\sin \hat{\theta} & \cos \hat{\theta} & 0 \end{bmatrix}^\top \\ {}^G\mathbf{n}_2^\perp &= \begin{bmatrix} -\cos \hat{\theta} \sin \hat{\phi} & -\sin \hat{\theta} \sin \hat{\phi} & \cos \hat{\phi} \end{bmatrix}^\top \end{aligned}$$

It is not difficult to see that the aided INS with a plane feature will have at least 6 unobservable directions:

$$\mathbf{N}_\pi = [\mathbf{N}_{\pi 1} \quad \mathbf{N}_{\pi 2:4} \quad \mathbf{N}_{\pi 5:6}] \quad (46)$$

$$= \begin{bmatrix} {}^I_1 \hat{\mathbf{R}}^G \mathbf{g} & \mathbf{0}_{3 \times 1} \\ \mathbf{0}_{3 \times 1} & \mathbf{0}_{3 \times 1} \\ -[{}^G \hat{\mathbf{V}}_{I_1} \times] {}^G \mathbf{g} & \mathbf{0}_{3 \times 1} & \mathbf{0}_{3 \times 1} & \mathbf{0}_{3 \times 1} & {}^G \hat{\mathbf{n}}_1^\perp & {}^G \hat{\mathbf{n}}_2^\perp \\ \mathbf{0}_{3 \times 1} & \mathbf{0}_{3 \times 1} \\ -[{}^G \hat{\mathbf{P}}_{I_1} \times] {}^G \mathbf{g} & {}^G \hat{\mathbf{n}}_1^\perp & {}^G \hat{\mathbf{n}}_2^\perp & {}^G \hat{\mathbf{n}}_\Pi & \mathbf{0}_{3 \times 1} & \mathbf{0}_{3 \times 1} \\ -g & 0 & 0 & 0 & 0 & 0 \\ 0 & 0 & 0 & 0 & 0 & 0 \\ 0 & 0 & 0 & -1 & 0 & 0 \end{bmatrix}$$

Note that $\mathbf{N}_{\pi 1}$ relates to the rotation around the gravitational direction, $\mathbf{N}_{\pi 2:4}$ relates to the sensor's global translation while $\mathbf{N}_{\pi 5:6}$ relates to the sensor motion perpendicular to the plane's normal direction.

B. Observability Analysis: Multiple Planes

Assuming that there are $m > 1$ plane features in the state vector, we define the orientation of the plane i and the rotation between plane i and plane j ($i, j \in \{1, \dots, m\}$) as:

$$\Pi_i \hat{\mathbf{R}} = [{}^G \hat{\mathbf{n}}_{\Pi i 1}^\perp \quad {}^G \hat{\mathbf{n}}_{\Pi i 2}^\perp \quad {}^G \hat{\mathbf{n}}_{\Pi i i}] \quad (47)$$

$$\Pi_j \hat{\mathbf{R}} = {}^G \hat{\mathbf{R}}_{\Pi i}^\top {}^G \hat{\mathbf{R}}_{\Pi j} \quad (48)$$

Lemma 3. For aided INS system with m plane features in the state vector,

- If $m = 2$ and the planes are not parallel, the system will have at least 5 unobservable directions.
- If $m \geq 3$ and these planes' intersections are not parallel, the system will have at least 4 unobservable directions.

Proof. See [28]. \square

VI. SIMULATION RESULTS

To validate our observability analysis, we perform 100 Monte Carlo simulations of visual-inertial odometry (VIO) using point [13], line and plane features, respectively. The simulated trajectory and different geometric features are shown in Fig. 1, where we assume a stereo camera with IMU is moving on spacial sine trajectories to get the feature measurements. In the results presented below, we implemented the MSCKF [13] as the VIO estimator to validate our observability analysis, since the MSCKF has been widely used for VINS with point features and its observability analysis has been well understood [1], [2]. In particular, we have compared two different versions of MSCKF: (i) the *ideal* MSCKF which uses true states as the linearization points and was shown to have correct observability properties and thus being consistent, and (ii) *standard* MSCKF which uses current state estimates as the linearization points and was found to be overconfident (inconsistent) [1], [2]. We compute the root mean squared error (RMSE) and the normalized estimation error squared (NEES) to quantify estimation accuracy and consistency [30]. The results are shown in Fig. 1. It is clear that the standard MSCKF performs worse than the ideal MSCKF which is consistent (though the comparison of orientation estimates is not as apparent

as position estimates). This implies the importance of understanding system observability properties for the design of consistent INS state estimators.

VII. CONCLUSIONS AND FUTURE WORK

We have performed observability analysis for INS aided by generic range and/or bearing measurements with different geometric features including points, lines and planes, which encapsulates the vision-aided INS as a special case. In particular, in the case of point features, we have systematically investigated the effects of global measurements on the aided INS observability and as expected, we found that the global measurements improve the system observability. Moreover, we have also identified four types of degenerate motion which should be avoided when performing aided INS. We further generalized the observability analysis to the aided INS with line and plane features, respectively, analytically proved that there exist at least 5 (6) unobservable directions with a single line (plane) feature, and for the first time, derived the unobservable directions for multiple lines or planes. The analysis is validated in the MSCKF-based VIO Monte Carlo simulations. In the future, we will leverage the presented observability analysis to design consistent estimators for different aided INS with geometric features.

REFERENCES

- [1] J. Hesch, D. Kottas, S. Bowman, and S. Roumeliotis, "Consistency analysis and improvement of vision-aided inertial navigation," *IEEE Transactions on Robotics*, vol. PP, no. 99, pp. 1–19, 2013.
- [2] ———, "Camera-IMU-based localization: Observability analysis and consistency improvement," *International Journal of Robotics Research*, vol. 33, pp. 182–201, 2014.
- [3] M. Li and A. I. Mourikis, "High-precision, consistent EKF-based visual-inertial odometry," *International Journal of Robotics Research*, vol. 32, no. 6, pp. 690–711, 2013.
- [4] S. Leutenegger, S. Lynen, M. Bosse, R. Siegwart, and P. Furgale, "Keyframe-based visual-inertial odometry using nonlinear optimization," *International Journal of Robotics Research*, Dec. 2014.
- [5] G. Huang, M. Kaess, and J. Leonard, "Towards consistent visual-inertial navigation," in *Proc. of the IEEE International Conference on Robotics and Automation*, Hong Kong, China, May 31–Jun. 7, 2014, pp. 4926–4933.
- [6] T. Qin, P. Li, and S. Shen, "Vins-mono: A robust and versatile monocular visual-inertial state estimator," *arXiv preprint arXiv:1708.03852*, 2017.
- [7] R. Mur-Artal and J. D. Tardós, "Visual-inertial monocular slam with map reuse," *IEEE Robotics and Automation Letters*, vol. 2, no. 2, pp. 796–803, 2017.
- [8] K. Eckenhoff, P. Geneva, and G. Huang, "Direct visual-inertial navigation with analytical preintegration," in *IEEE International Conference on Robotics and Automation*. IEEE, 2017, pp. 1429–1435.
- [9] J. Zhang and S. Singh, "Enabling aggressive motion estimation at low-drift and accurate mapping in real-time," in *International Conference on Robotics and Automation*. IEEE, 2017, pp. 5051–5058.
- [10] C. X. Guo and S. I. Roumeliotis, "Imu-rgbd camera navigation using point and plane features," in *International Conference on Intelligent Robots and Systems*, Tokyo, Japan, Nov. 3–7, 2013, pp. 3164–3171.
- [11] Y. Yang and G. Huang, "Acoustic-inertial underwater navigation," in *2017 IEEE International Conference on Robotics and Automation (ICRA)*. IEEE, 2017.
- [12] G. Huang, A. I. Mourikis, and S. I. Roumeliotis, "Observability-based rules for designing consistent EKF SLAM estimators," *International Journal of Robotics Research*, vol. 29, no. 5, pp. 502–528, Apr. 2010.
- [13] A. I. Mourikis and S. I. Roumeliotis, "A multi-state constraint Kalman filter for vision-aided inertial navigation," in *International Conference on Robotics and Automation*, Rome, Italy, Apr. 10–14, 2007, pp. 3565–3572.

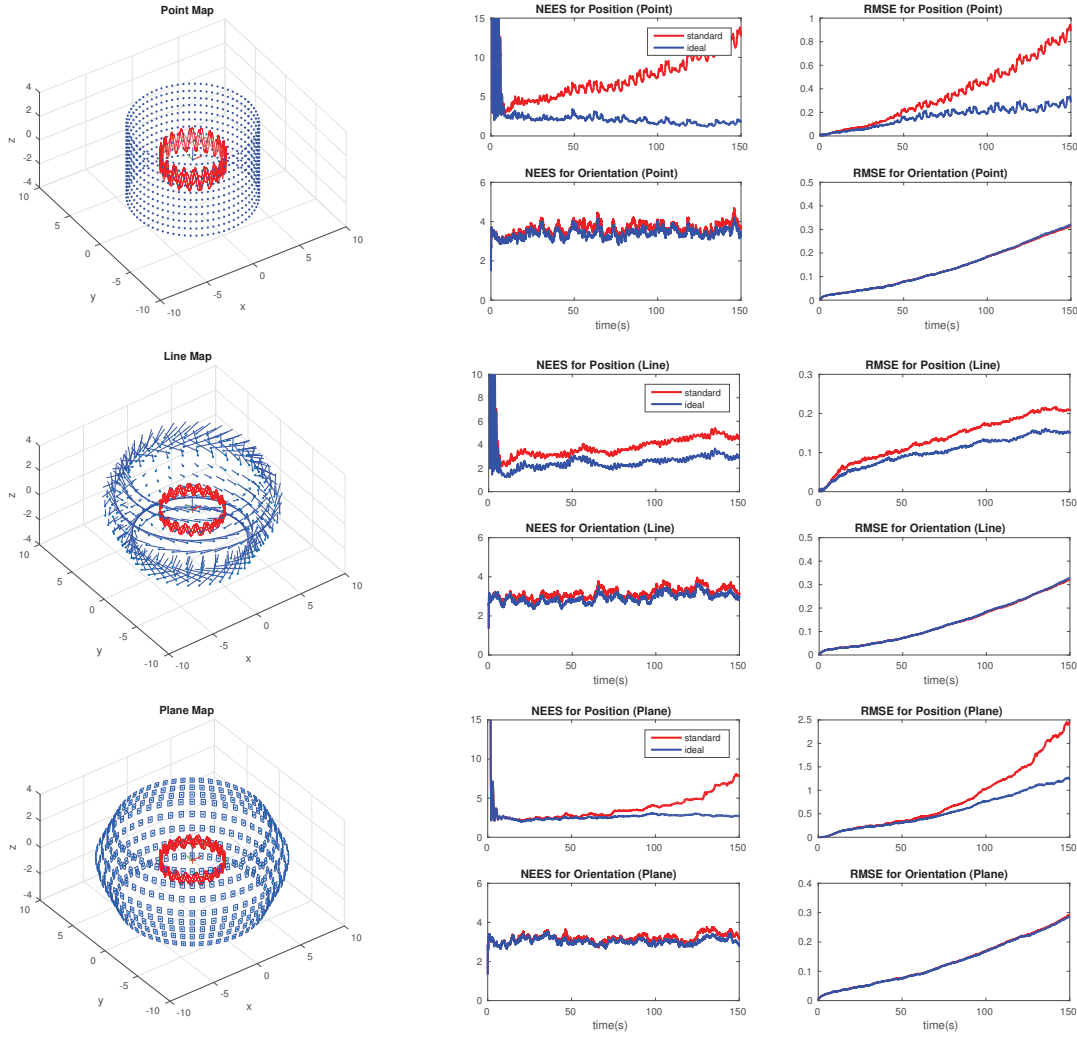


Fig. 1. Monte Carlo results of the standard and ideal MSCKFs for different geometric features: (top) points, (middle) lines, and (bottom) planes.

- [14] G. Huang, "Improving the consistency of nonlinear estimators: Analysis, algorithms, and applications," Ph.D. dissertation, Department of Computer Science and Engineering, University of Minnesota, 2012.
- [15] E. S. Jones and S. Soatto, "Visual-inertial navigation, mapping and localization: A scalable real-time causal approach," *International Journal of Robotics Research*, vol. 30, no. 4, pp. 407–430, Apr. 2011.
- [16] J. Hernandez, K. Tsotsos, and S. Soatto, "Observability, identifiability and sensitivity of vision-aided inertial navigation," in *IEEE International Conference on Robotics and Automation*. IEEE, 2015, pp. 2319–2325.
- [17] A. Martinelli, "Vision and IMU data fusion: Closed-form solutions for attitude, speed, absolute scale, and bias determination," *IEEE Transactions on Robotics*, vol. 28, no. 1, pp. 44–60, 2012.
- [18] ———, "Visual-inertial structure from motion: Observability and resolvability," in *2013 International Conference on Intelligent Robots and Systems*, Tokyo, Japan, Nov 2013, pp. 4235–4242.
- [19] D. G. Kottas, J. A. Hesch, S. L. Bowman, and S. I. Roumeliotis, "On the consistency of vision-aided inertial navigation," in *International Symposium on Experimental Robotics*, Quebec City, Canada, Jun. 17–20, 2012.
- [20] R. Hermann and A. Krener, "Nonlinear controllability and observability," *IEEE Transactions on Automatic Control*, vol. 22, no. 5, pp. 728 – 740, Oct. 1977.
- [21] C. Guo and S. Roumeliotis, "IMU-RGBD camera 3D pose estimation and extrinsic calibration: Observability analysis and consistency improvement," in *Proc. of the IEEE International Conference on Robotics and Automation*, Karlsruhe, Germany, May 6–10, 2013.
- [22] K. J. Wu, C. X. Guo, G. Georgiou, and S. I. Roumeliotis, "Vins on wheels," in *2017 IEEE International Conference on Robotics and Automation*. IEEE, 2017, pp. 5155–5162.
- [23] H. Yu and A. I. Mourikis, "Vision-aided inertial navigation with line features and a rolling-shutter camera," in *International Conference on Robotics and Intelligent Systems*, Hamburg, Germany, October 2015, pp. 892–899.
- [24] G. Panahandeh, C. X. Guo, M. Jansson, and S. I. Roumeliotis, "Observability analysis of a vision-aided inertial navigation system using planar features on the ground," in *International Conference on Intelligent Robots and Systems*. IEEE, 2013, pp. 4187–4194.
- [25] D. G. Kottas and S. I. Roumeliotis, "Efficient and consistent vision-aided inertial navigation using line observations," in *IEEE International Conference on Robotics and Automation*, Karlsruhe, Germany, May 6–10 2013, pp. 1540–1547.
- [26] A. Bartoli and P. Sturm, "Structure from motion using lines: Representation, triangulation and bundle adjustment," *Computer Vision and Image Understanding*, vol. 100, no. 3, pp. 416–441, dec 2005.
- [27] N. Trawny and S. I. Roumeliotis, "Indirect Kalman filter for 3D attitude estimation," University of Minnesota, Dept. of Comp. Sci. & Eng., Tech. Rep., Mar. 2005.
- [28] Y. Yang and G. Huang, "Aided inertial navigation with geometric features: Observability analysis," RPNG, University of Delaware, Tech. Rep., 2017, link: udel.edu/~yuyang/downloads/tr_observability.pdf.
- [29] X. Zuo, X. Xie, Y. Liu, and G. Huang, "Robust visual slam with point and line features," in *International Conference on Intelligent Robots and Systems*, Vancouver, Canada, Sep. 2017.
- [30] Y. Bar-Shalom and T. E. Fortmann, *Tracking and Data Association*. New York: Academic Press, 1988.